Supplementary Information for

Effect of In-Plane Aspect Ratio of Graphene Filler on Anisotropic Heat Conduction in Paraffin/Graphene Composite

Hiroki Matsubara*,[a] and Taku Ohara[a]

[a]Institute of Fluid Science, Tohoku University, 2-1-1 Katahira, Aoba-ku, Sendai 980-8577, Japan

*Corresponding author: E-mail: matsubara@microheat.ifs.tohoku.ac.jp

In this supplemental information, we describe the computational procedures for the properties of the paraffin matrix and graphene fillers used in the present study in section S1 and S2. The simulation settings not explicitly written here are the same as those of the composite simulations explained in section 2.2 in the main text. In addition, figures to support the description in the main text are included in section S3, S4, and S5.

S1. Thermal conductivity of a single-layer graphene

Thermal conductivity of a single-layer graphene (SLG) sheet in a vacuum was calculated for the square and ribbonlike graphene fillers using non-equilibrium molecular dynamics (NEMD) simulation under steady heat conduction. The simulation setup for the square filler is illustrated in Fig. S1. The setup for the ribbonlike filler is much the same. The graphene sheet was placed inside an MD box with the free boundary conditions in all *x*, *y*, and *z* directions, so that the longer edge is parallel to the heat conduction direction (the *z* direction). The square and ribbonlike fillers used in the NEMD simulations were elongated in the heat conduction direction by 3.0 nm so that the regions 1.5 nm from the left and right armchair edges were used for the hot and cold heat sources. In addition, the outermost C and H atoms in the shorter edges were frozen throughout the simulation.

After all graphene atoms except the frozen ones were equilibrated at 360 K with an *NVT* run for 2.5 ns, a steady state under constant temperature gradient was reached by a 5 ns run, where the temperature of the hot and cold heat sources were controlled to 365 K and 355 K, respectively, using the Langevin thermostat while the atoms in other regions followed the *NVE* dynamics. The production run was then continued for 50 ns. During the production run, the temperature profile along the heat conduction direction was calculated at 2.0 Å interval. The average heat flux applied to the control volume, J_Q, was calculated from the average rate of energy injected to the hot source, $\dot{e}_+$, and that removed from the cold source, $\dot{e}_-$, as $J_Q = (\dot{e}_+ - \dot{e}_-)/(2l_2l_3)$, where l_2 is the length of the shorter edge. The effective thickness of an SLG, l_3, was approximated to be 3.4 Å following other MD studies [1,2]. The value of temperature gradient $\nabla_z T$ was obtained from a linear fit to the temperature profile within the control volume that was placed 4 Å apart from the hot and cold sources. Finally, thermal conductivity was derived using the Fourier law as $\lambda = -J_Q/\nabla_z T$. The thermal conductivity thus obtained for a single-layer square filler was 54 ± 5 W/(m·K) with J_Q = 52.2 ± 0.8 GW/m^2

whereas that for the ribbonlike filler was 66 ± 4 W/(m·K) with J_Q = 31 ± 1 GW/m^2. Thus, the ribbonlike filler has a higher thermal conductivity than the square filler with the relative difference of 22%. Our results were consistent with literature values 46–78 W/(m·K) calculated for nanographenes with similar surface area (~2 × 10 nm^2) using the AIREBO potential [3].

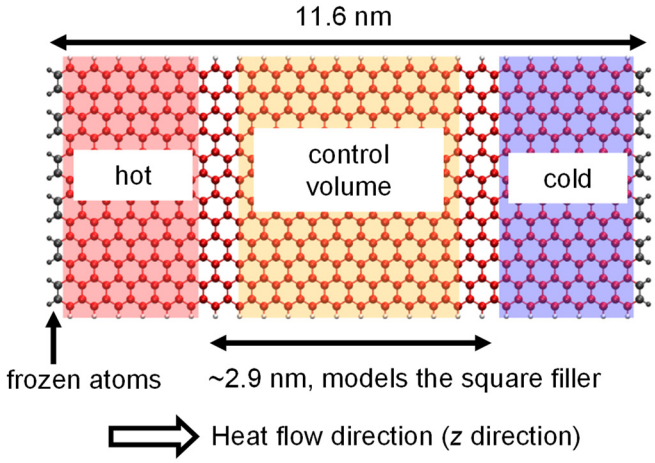

Fig. S1. Setup for the NEMD simulation for a single sheet of the square graphene filler in a vacuum.

S2. Phase change properties of nonacosane

Although melting temperature T_m can be estimated by simply heating or cooling a system at a certain rate, this method usually suffers from a hysteresis that melting and freezing occur at different temperature points [4]. Here, to avoid the hysteresis, we used the local equilibrium NEMD (LE-NEMD) scheme [5] to determine the melting temperature T_m and the specific enthalpy of fusion, Δh, of nonacosane. This scheme conducts a single run of NEMD simulation under steady heat conduction to evaluates equilibrium properties at different temperature conditions on the basis of the local equilibrium hypothesis. We constructed the system of LE-NEMD simulation as illustrated in Fig. S2(a), where we chose the z direction as the heat conduction direction. The crystalline phase of nonacosane just below T_m is called the R-IV

rotator phase. In this phase, molecules align parallel, but there is no order in the molecular orientation about the molecular axis [6]. Therefore, we started from an initial configuration where 2752 nonacosane molecules were aligned in a face-centered-cubic (fcc) structure in the manner that all molecules were parallel to the y direction. These molecules were put in a rectangular MD box whose initial dimensions were $80 \times 73 \times 338$ Å^3 and the periodic boundary conditions were imposed on all x, y, and z directions. The fcc crystal state was equilibrated by a 2.5 ns NpT run at 260 K and 1 atm, where the x, y, and z lengths of MD box were relaxed independently. Next, the NEMD run of steady heat conduction was performed for 65 ns using the NpH (isobaric-isoenthalpy) dynamics, where the hot and cold heat sources were controlled by velocity scaling to 420 K and 260 K, respectively. During the NEMD run, the geometries of the MD box were fixed except the position of the right end in the z direction so that only the z length can be relaxed. As shown in Fig. S2(a), the system was partly melted to make a solid–liquid interface. From the last 25 ns of the NEMD run, the local profile of temperature $T(z)$ and specific enthalpy $h(z)$ were computed at the interval of $\Delta z = 0.478$ nm. The former is shown in the bottom panel of Fig. S2(a). In the analysis below, the local profiles of $T(z)$ and $h(z)$ were considered only for the z values greater than the right end of the cold slab ($z \geq 14$ nm).

As shown in Fig. S2(b), a jump was seen when $h(z)$ was plotted as a function of $T(z)$. Numerical differentiation of this plot gave the specific heat at constant pressure, $c_p = \partial h/\partial T$, which showed a peak as a function of temperature as shown in Fig. S2(c). This peak was approximated by a gaussian of the form $A\exp[-(T-T_\mathrm{m})^2/B]+C$ with A, B, C, and melting temperature T_m being fitting parameters, from which $T_\mathrm{m} = 348$ K was determined. Then, back to Fig. S2(b), enthalpy of fusion was determined to be $\Delta h = 83.9$ kJ/mol as the difference at T_m between the two linear extrapolations of $h(T)$ from the solid and liquid sides. The simulated melting temperature was well compared with the experimental one [7], $T_\mathrm{m} = 336.8$ K, although the simulated enthalpy of fusion was somewhat higher than the experimental observation $\Delta h =$ 66.939 kJ/mol.

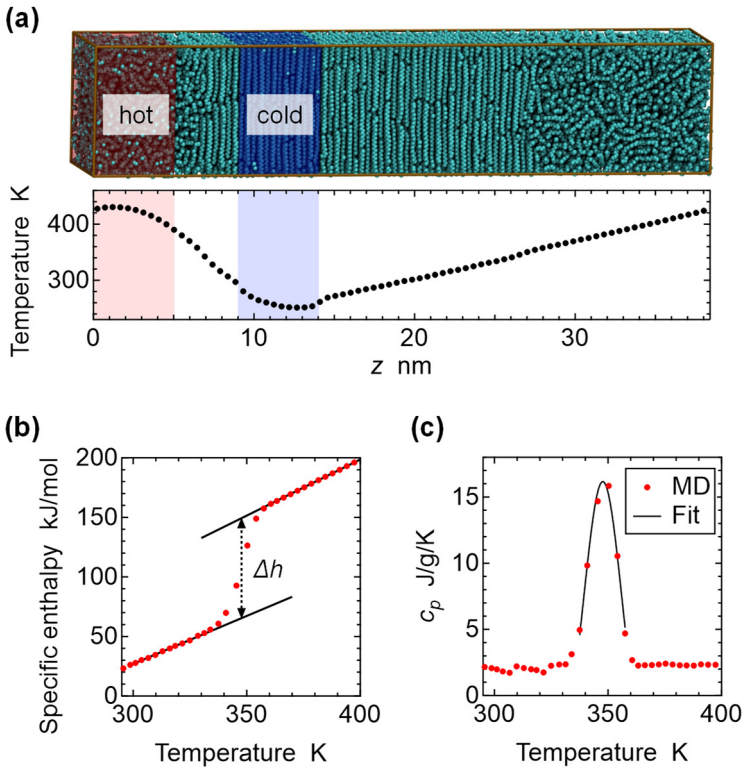

Fig. S2. Summary of our LE-NEMD simulation to determine the phase change properties of nonacosane. (a) MD system and temperature profile. The temperature dependence of (c) specific enthalpy and (d) specific heat.

S3. Example for the initial configuration of the composite system

As an example, we show the simulation snapshot of initial molecular arrangement for the case of 20 wt% rectangular fillers in Fig. S3(a). First, 1440 paraffin molecules were put at the lattice positions of an fcc crystal and in the same molecular orientation, so that they roughly uniformly fit into a cubic simulation box with 170Å on a side. Overlaid on this paraffin lattice, graphene sheets were aligned apart at a regular interval and in the same orientation so that its longest axis is parallel to the paraffin molecular axis. Then, a paraffin molecule was deleted if any C atom in the molecule overlapped with a graphene C atom within $(\sigma_{CP} + \sigma_{CG})/2$, where σ_{CP} and σ_{CG} are the distance parameters of the Lennard-Jones potential of C atoms in graphene and paraffin, respectively. Finally, the number of graphene sheets and paraffin molecules were fine-tuned so as the filler mass fraction to be close to the desired value.

Fig. S3(b) illustrates the snapshot during the *NpT* simulation at 600 K for agitation, where the memory of the initial configuration appears to be erased. This configuration in the middle of relaxation stage is also different from the final state at 360 K displayed in Figs. 1(e) and 1(f) in the main text and Fig. S4(b). Thus, the high orientational order of ribbonlike filler at the final state is not the artifact of the initial molecular arrangement.

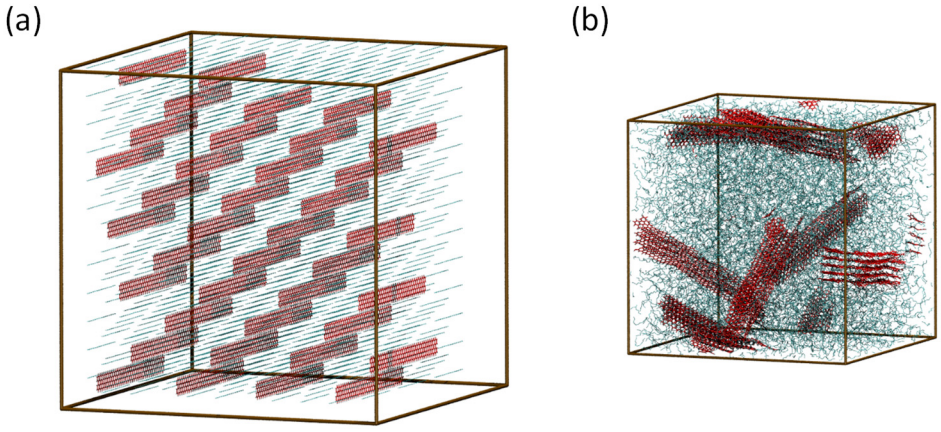

Fig. S3. Simulation snapshots for the system with 20 wt% ribbonlike fillers (a) at the initial configuration and (b) at the agitation stage at 600 K (2.0 ns after the initial configuration). Figs. (a) and (b) are displayed in the same scale.

S4. Simulation snapshots all systems.

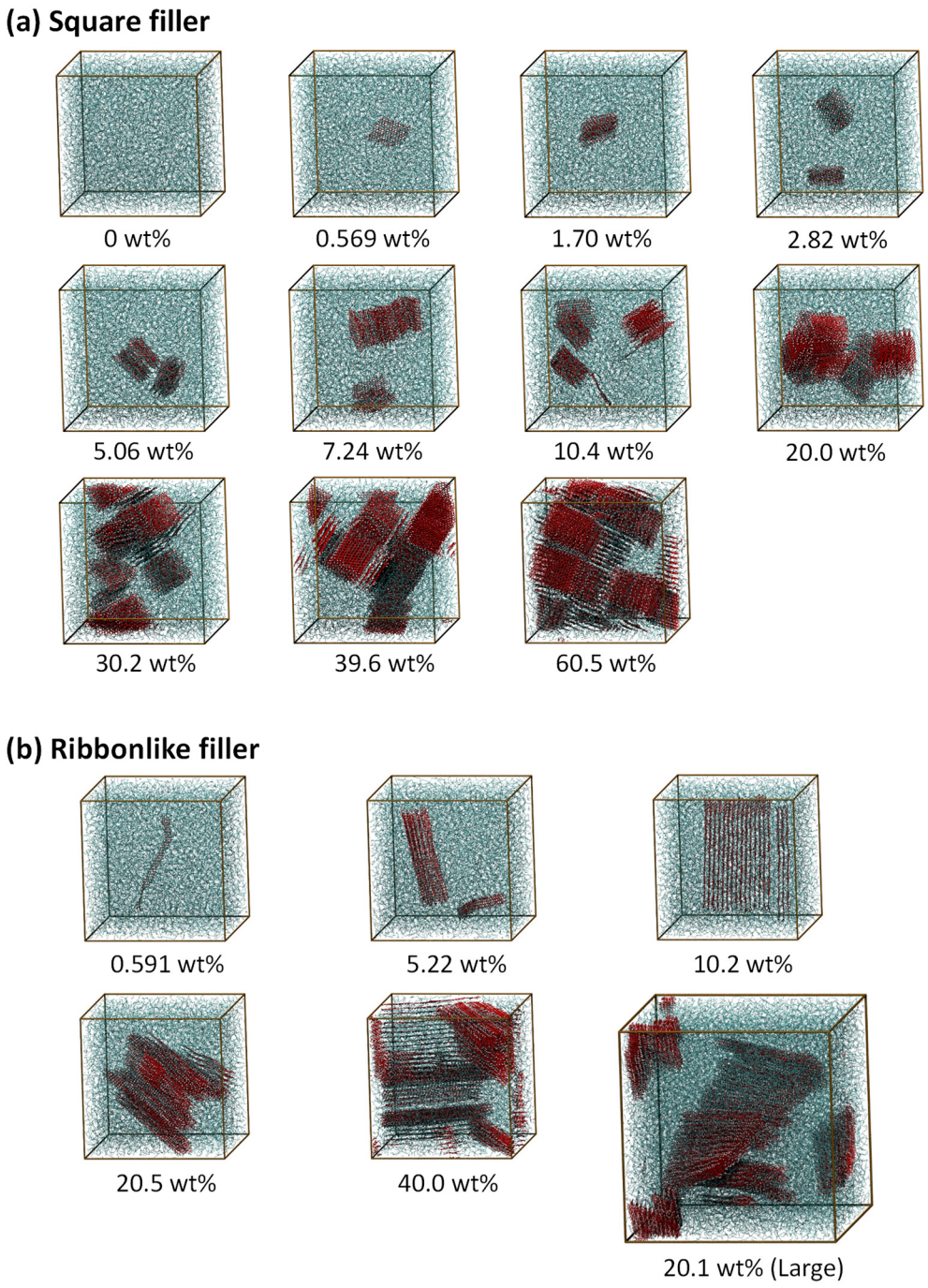

Fig. S4. Simulation snapshots for systems with (a) square filler and (b) ribbonlike filler examined in the present study. The snapshot of the larger system with 20 wt% ribbonlike fillers is also shown.

S5. Thermal conductivity decomposition in terms of the absolute value

In the main text, Fig. 6 shows the partial thermal conductivity as the percentage to the total thermal conductivity. For reference, the same data is plotted in terms of the absolute value in Fig. S5.

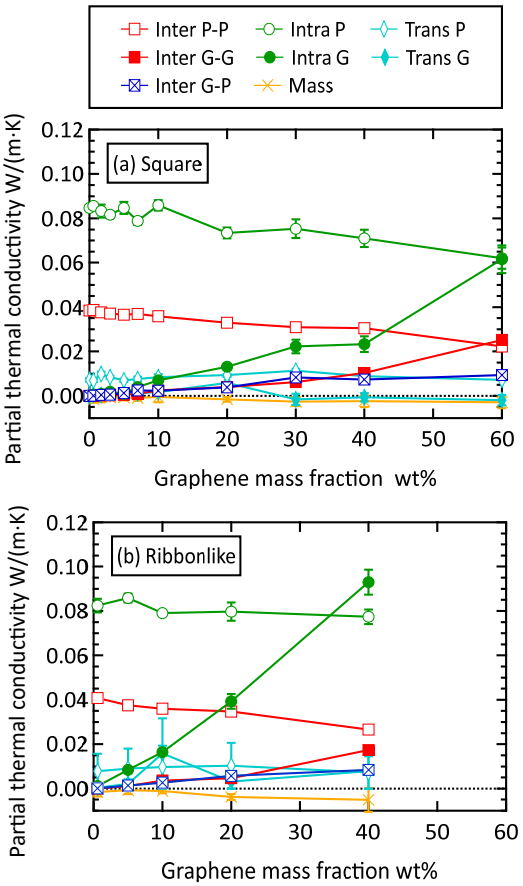

Fig. S5. Decomposition of the isotropic thermal conductivity of the paraffin/graphene composite with (a) square filler and (b) ribbonlike filler. The total thermal conductivity was decomposed into contributions from the thermal energy transfer associated with intermolecular interaction (Inter), intramolecular interaction (Intra), molecular transport (Trans), and heat–mass coupling (Mass), and P and G indicate paraffin and graphene, respectively.

References

[1] Z. Fan, L.F.C. Pereira, H.-Q. Wang, J.-C. Zheng, D. Donadio, A. Harju, Force and heat current formulas for many-body potentials in molecular dynamics simulations with applications to thermal conductivity calculations, Phys. Rev. B. 92 (2015) 94301. doi:10.1103/PhysRevB.92.094301.

[2] S. Srinivasan, M.S. Diallo, S.K. Saha, O.A. Abass, A. Sharma, G. Balasubramanian, Effect of temperature and graphite particle fillers on thermal conductivity and viscosity of phase change material n-eicosane, Int. J. Heat Mass Transf. 114 (2017) 318–323. doi:10.1016/j.ijheatmasstransfer.2017.06.081.

[3] C. Si, X.D. Wang, Z. Fan, Z.H. Feng, B.Y. Cao, Impacts of potential models on calculating the thermal conductivity of graphene using non-equilibrium molecular dynamics simulations, Int. J. Heat Mass Transf. 107 (2017) 450–460. doi:10.1016/j.ijheatmasstransfer.2016.11.065.

[4] H. Babaei, P. Keblinski, J.M. Khodadadi, Thermal conductivity enhancement of paraffins by increasing the alignment of molecules through adding CNT/graphene, Int. J. Heat Mass Transf. 58 (2013) 209–216. doi:http://dx.doi.org/10.1016/j.ijheatmasstransfer.2012.11.013.

[5] H. Matsubara, G. Kikugawa, T. Bessho, S. Yamashita, T. Ohara, Non-equilibrium molecular dynamics simulation as a method of calculating thermodynamic coefficients, Fluid Phase Equilib. 421 (2016) 1–8. doi:http://dx.doi.org/10.1016/j.fluid.2016.03.019.

[6] E.B. Sirota, H.E. King, D.M. Singer, H. Shao, A synchrotron X-ray scattering study of the rotator phases of the normal alkanes, J. Phys. D. Appl. Phys. 26 (1993) B133–B136. doi:10.1088/0022-3727/26/8B/021.

[7] V. Chevallier, M. Bouroukba, D. Petitjean, D. Barth, P. Dupuis, M. Dirand, Temperatures and enthalpies of solid-solid and melting transitions of the odd-numbered n-alkanes C21, C23, C25, C27, and C29, J. Chem. Eng. Data. 46 (2001) 1114–1122. doi:10.1021/je0003501.